Potential Vorticity Distribution along CALCOFI Line 67

LCDR David M. Ruth

Winter 2001

Naval Postgraduate School
Code 35
Monterey, CA 93943-5114

dmruth@nps.navy.mil

Operational Oceanography
OC3570

Potential Vorticity Distribution along CALCOFI Line 67

1. Introduction

Potential vorticity has been shown to be useful in studies of large-scale ocean circulation. In an ideal fluid, potential vorticity is a conserved quantity, and the fundamental equation governing the evolution of large-scale ocean circulation is the potential vorticity equation. Keffer (1985) maps potential vorticity within four different density layers for the North and South Atlantic, North and South Pacific, and Indian Oceans, and uses these maps to evaluate the character of the thermocline of the world's oceans. Talley and McCartney (1982) infer the circulation of Labrador Sea Water at mid-depths in the North Atlantic using potential vorticity as a water mass tracer. Talley (1988) presents vertical sections and maps of potential vorticity to give a three-dimensional picture of circulation in the North Pacific Ocean.

In this study, a smaller horizontal scale (O(100km)) is considered. Potential vorticity is computed and contoured along CALCOFI Line 67, and the structure of the water column along this transect is observed.

2. Methods

a. Collection

Conductivity-Temperature-Depth (CTD) data were obtained along CALCOFI Line 67 from a survey conducted by the *R/V Point Sur* during the period 4-8 December 2000. A Seabird 911 Plus CTD was used to measure vertical profiles of temperature and conductivity at 20 stations along the survey line (Figure 1). Each station was sampled at 2 dbar intervals, and data were analyzed to 1000 dbar (except for the easternmost station, where the CTD cast only descended to 242 dbar). Additionally, Acoustic Doppler

Current Profiler (ADCP) measurements were taken at 39 locations along the Line 67 transect; cross-shore and alongshore current data were averaged over 10m increments from 20m down to the bottom (or to about 400m, whichever was shallower).

b. Analysis

MATLAB 5.3 was used for all data extraction, computation, and plotting. For each station, raw CTD data values were scanned and plots were inspected for "bad" data points (none were identified). A Hanning forward-and-backward filter was applied to smooth the data. Several filter widths were considered; the final width used for analysis (a 50-point filter for each 500-point data set) was chosen as the best compromise of feature resolution and noise suppression.

Potential vorticity, $(f/\rho)d\rho/dz$, was directly computed for each station using the "Buoyancy (Brunt-Väisälä) Frequency" routine in MATLAB's SEAWATER library. Plots and contours of temperature, salinity, density anomaly, and potential vorticity were produced to evaluate the vertical structure along the sampled section as discussed below. The "truncation" of all the plots at the easternmost station is due to the partial data set (121 vice 500 data points) at that location.

ADCP data, already averaged in the available data set, were smoothed using MATLAB's "*pcolor*" and "*interp*" features, and alongshore current was plotted and evaluated in conjunction with the potential vorticity analysis.

AVHRR satellite imagery for the location and time of this experiment was also studied to identify any surface features with distinct sea surface temperature signatures. Cloud cover was very limiting during this time period, making only a few images useful for comparison with the other data.

3. Observations

a. Temperature and salinity

For small changes in latitude, the influential variable in the calculation of potential vorticity is the fractional change in density with depth, $\rho^{-1}d\rho/dz$. Profiles (Figures 2 and 3) and contours (Figures 4 and 5) of temperature and salinity provide a glimpse of the overall density structure along the sample line. In general, the lowest surface temperatures and highest surface salinities are found closest to shore, with temperature increasing and salinity decreasing seaward (two anomalies in the surface salinity trend are discussed below). A strong thermocline is evident between 50 and 100 dbar; the halocline extends from about 50 to 150 dbar. At the station nearest to shore, the thermocline and halocline are weakest. Profiles of temperature and salinity statistics (Figure 6) show that horizontal variability of both parameters is greatest in the mixed layer. Contours of density anomaly (Figure 7) confirm the presence of a strong density gradient between 50 and 150 dbar west of 122˚W, as well as a weaker vertical density gradient closest to shore. From these observations, one would expect potential vorticity maxima at depths coinciding with the thermocline and halocline. Horizontal variability of potential vorticity, if any, should occur shallower than 150 dbar. Where the vertical density gradient is weakest (the easternmost stations), potential vorticity should be low.

b. Potential vorticity

Contours of potential vorticity (Figure 8, plotted down to 300 dbar) depict several features worthy of discussion. Most prominent is the potential vorticity "ridge" at about 60 dbar, with two well-defined local maxima in the vicinity of longitudes 123˚40'W and 125˚00'W. This ridge coincides with the steep vertical density gradient seen on the

temperature, salinity, and density anomaly plots. The potential vorticity graphic, however, makes it much easier to identify precisely where the density gradient is steepest (see overlay of potential vorticity and density anomaly contours, Figure 9). An interesting question is whether the two potential vorticity peaks are associated with any particular flow feature(s). The horizontal extent of the smaller peak is O(30km), while that of the larger is O(100km). Both peaks are larger than the internal Rossby radius of deformation ($R_i \approx$ 10km), and thus it is reasonable that these anomalies might identify a specific large-scale flow feature. Although no resolvable feature was evident in the study of several satellite images covering the location and time of this experiment, salinity contours and ADCP data both substantiate a flow anomaly associated with these peaks. Specifically, significant salinity minima (<33 psu, Figure 5) exist at shallow depths exactly above the locations of the potential vorticity maxima. These salinity minima might be expected as a result of advection of fresher surface water from the north. The ADCP data (Figure 10) confirm the presence of two anomalous cores of southward flow (>30 cm/s) in the upper 50 dbar above the potential vorticity maxima.

Little horizontal variation in potential vorticity exists shallower than 30 dbar and deeper than 200 dbar, as expected. Closest to shore (around 122˚W), potential vorticity is nearly constant with depth, in stark contrast to the strong ridge evident to the west along the rest of the section. Near-shore upwelling significantly reduces the vertical density gradient in the water column, and thus the vertical "flatness" of potential vorticity in the east serves as an indicator of both the strength and extent of this upwelling phenomenon.

4. Discussion

a. Data processing

An important objective of this study was to familiarize the student with the details and procedures of data collection and processing. The at-sea portion of this project gave me an immensely greater appreciation for the amount of work involved in obtaining a useful data set for study. Even more instructive was the task of meaningfully processing the data sets of interest. Some tasks were easier than expected: for example, the computation of potential vorticity was simplified by searching out and finding an existing MATLAB routine that performed the calculation directly. This prevented having to code a potential vorticity routine "from scratch." More difficult than expected was the manipulation of data in its raw form to a matrix form that could be used for computation. Another challenge was finding the appropriate filter width and contour interval to best smooth the temperature and salinity data and display the potential vorticity results. Many filter width and contour interval combinations were run to find which suppressed as much noise as possible without sacrificing the resolution of important features. The selection of an "optimal" combination was fairly subjective. In the end, this exercise provided or built upon several skills which will be vital for any future scientific research in which I am involved.

b. Results

While potential vorticity is perhaps not the most intuitive variable from which to infer ocean structure, the observations in this experiment highlight some utility of this parameter. Contours of potential vorticity quantitatively identify the distribution of density gradients in the water column. In this study, local maxima in the potential

vorticity field were correlated with flow features verified by salinity and current data. Vertical potential vorticity isopleths are expected where the water column is "well-ventilated," and in this study the column of nearly homogeneous potential vorticity corresponds precisely to an upwelling region. A possible area for further study would be to map potential vorticity with depth over some horizontal area of interest (for example, the area bound by 35N-38N and 122W-125W) and observe what three-dimensional structure is represented. Overall, this brief study suggests that potential vorticity analysis can be a useful approach to the study of ocean circulation, even at scales as small as O(100km).

REFERENCES

Keffer, T., 1985: The Ventilation of the World's Oceans: Maps of the Potential Vorticity Field. *J. Phys. Oceanogr.*, **15**, 509-523.

Talley, L.D., 1988: Potential Vorticity Distribution in the North Pacific. *J. Phys. Oceanogr.*, **18**, 89-106.

Talley, L.D., and McCartney, M.S., 1982: Distribution and Circulation of Labrador Sea Water. *J. Phys. Oceanogr.*, **12**, 1189-1205.

FIGURES

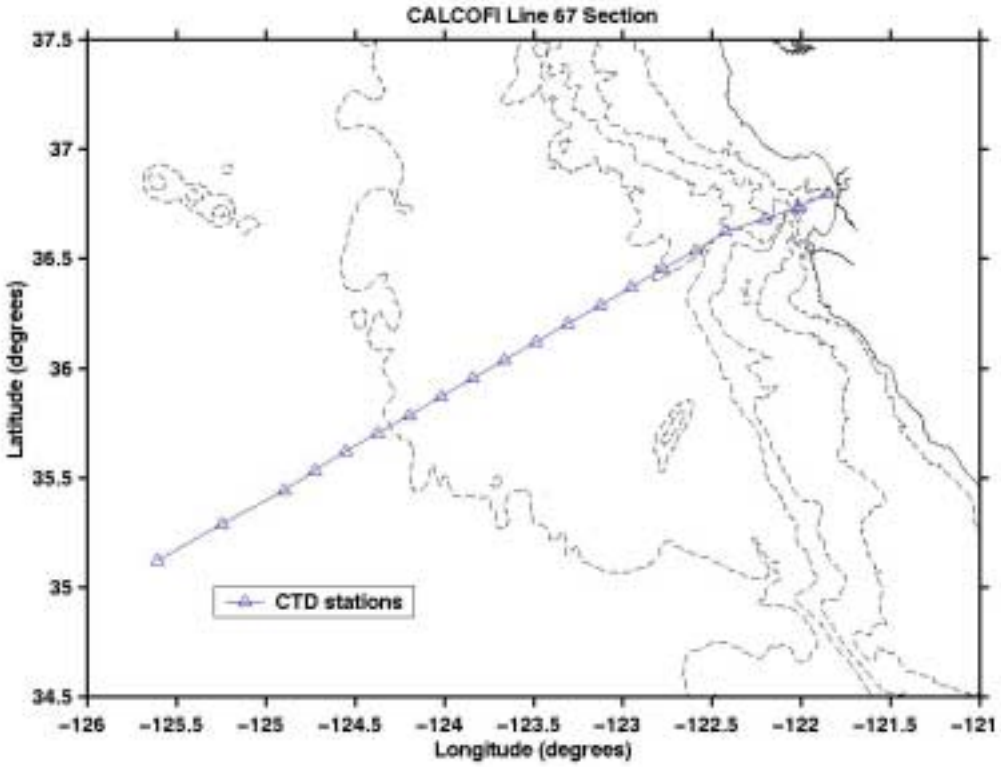

Figure 1. CALCOFI Line 67 CTD stations. Negative longitude values denote west longitude.

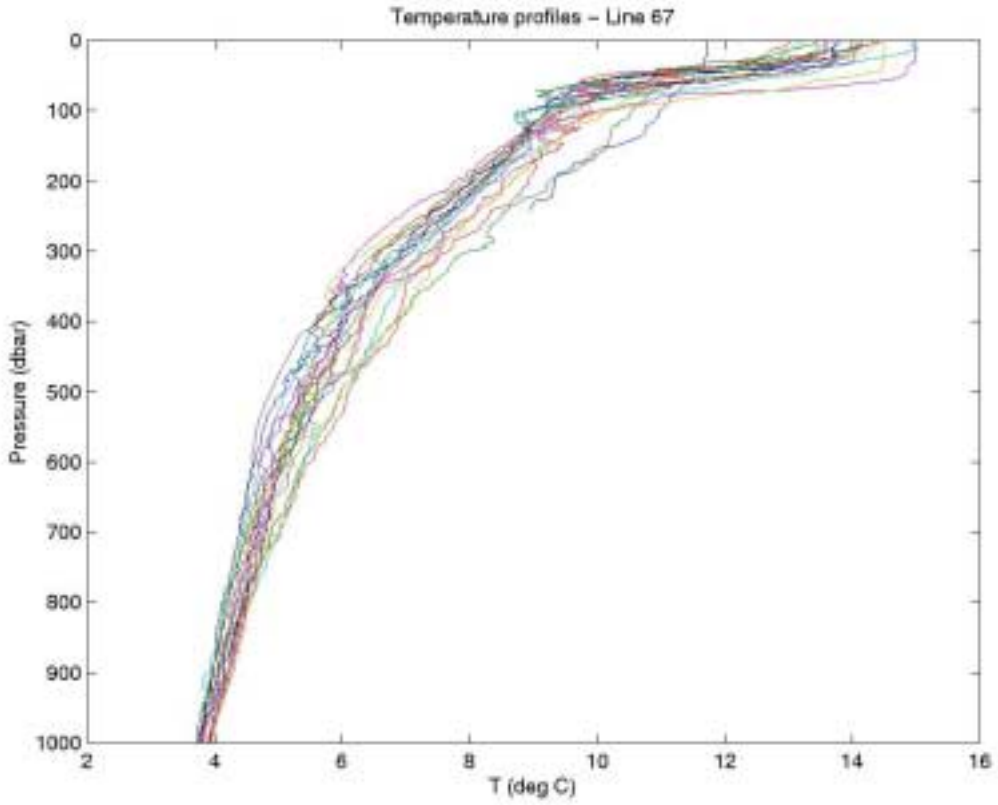

Figure 2. Temperature profiles for the 20 CTD stations along CALCOFI Line 67.

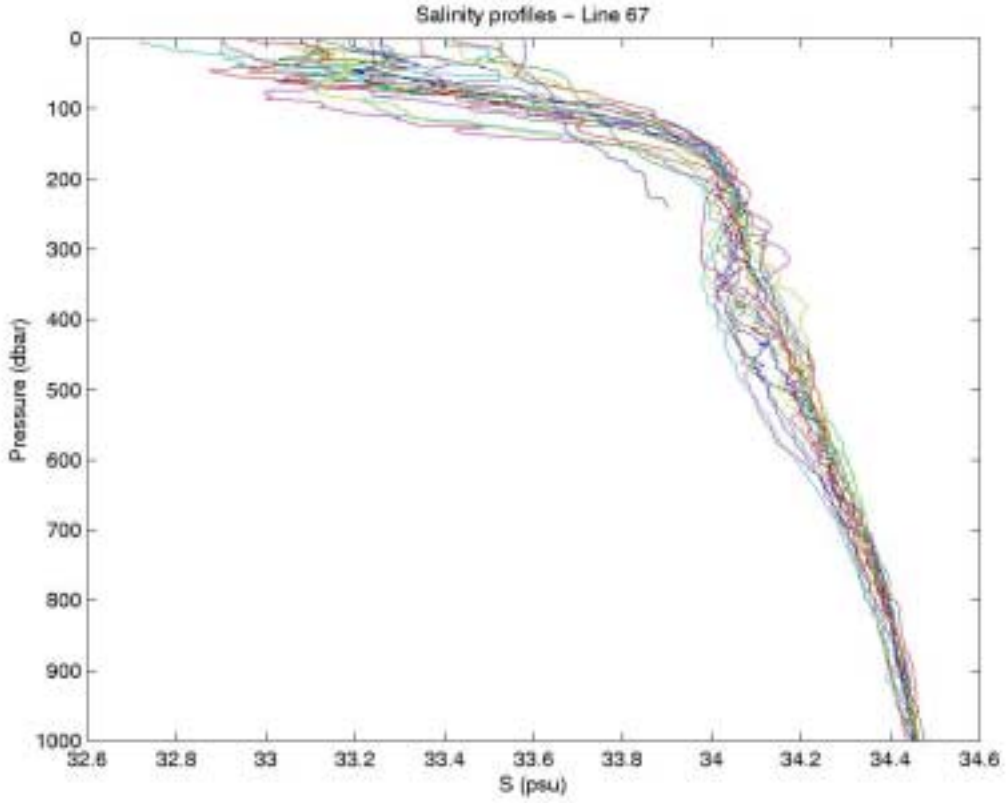

Figure 3. Salinity profiles for the 20 CTD stations along CALCOFI Line 67.

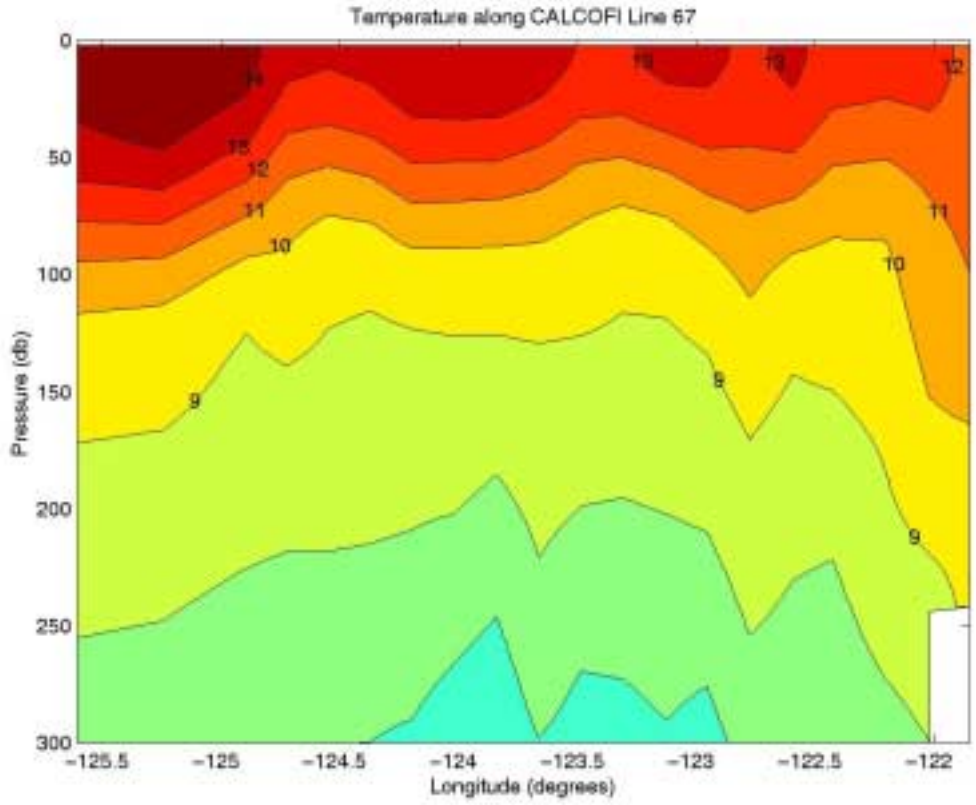

Figure 4. Temperature (˚C) along CALCOFI Line 67

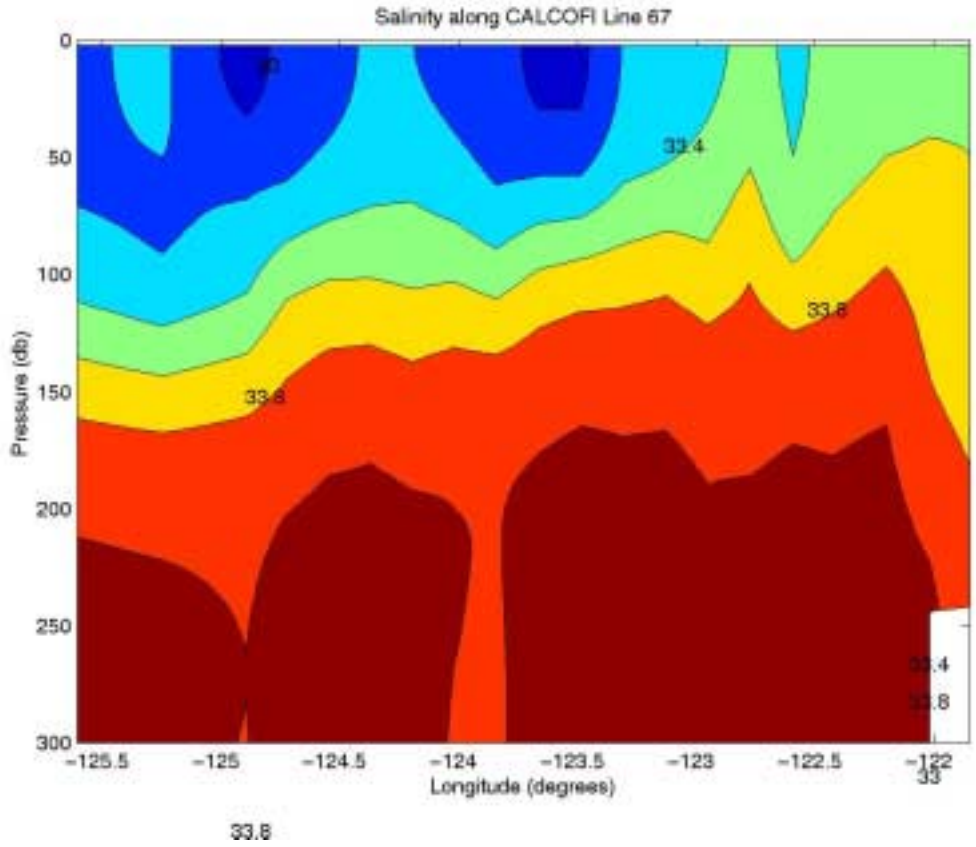

Figure 5. Salinity (psu) along CALCOFI Line 67

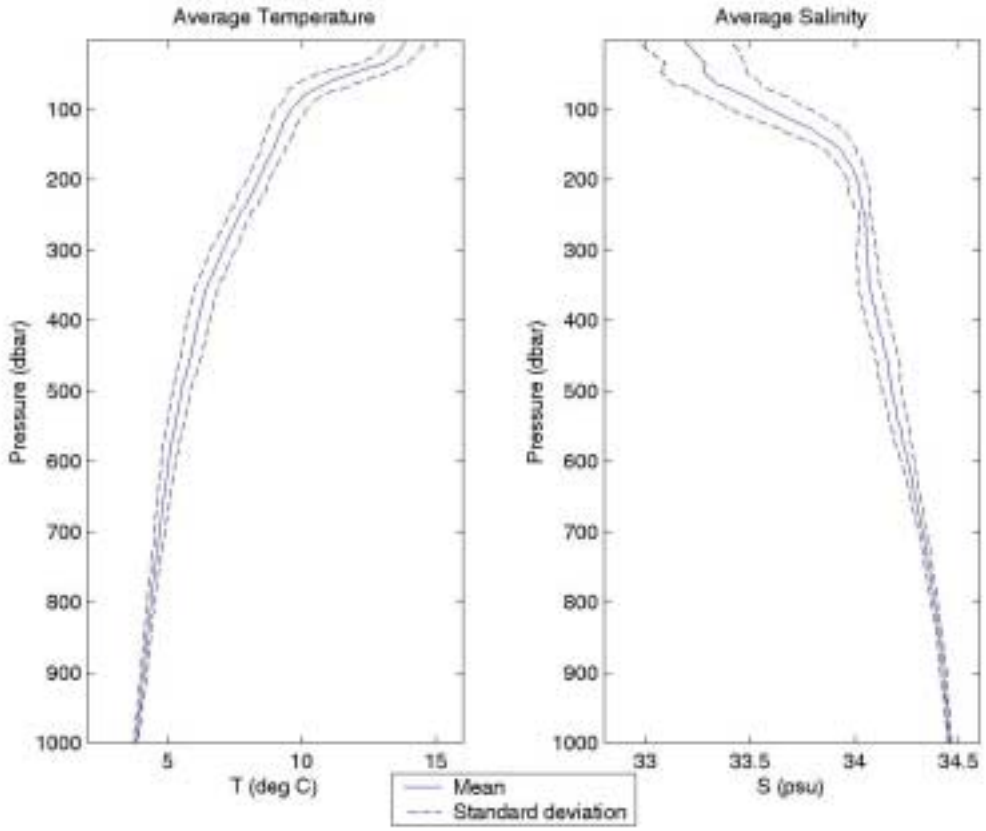

Figure 6. Mean temperature and salinity for CALCOFI Line 67. Dashed lines denote one standard deviation from the mean.

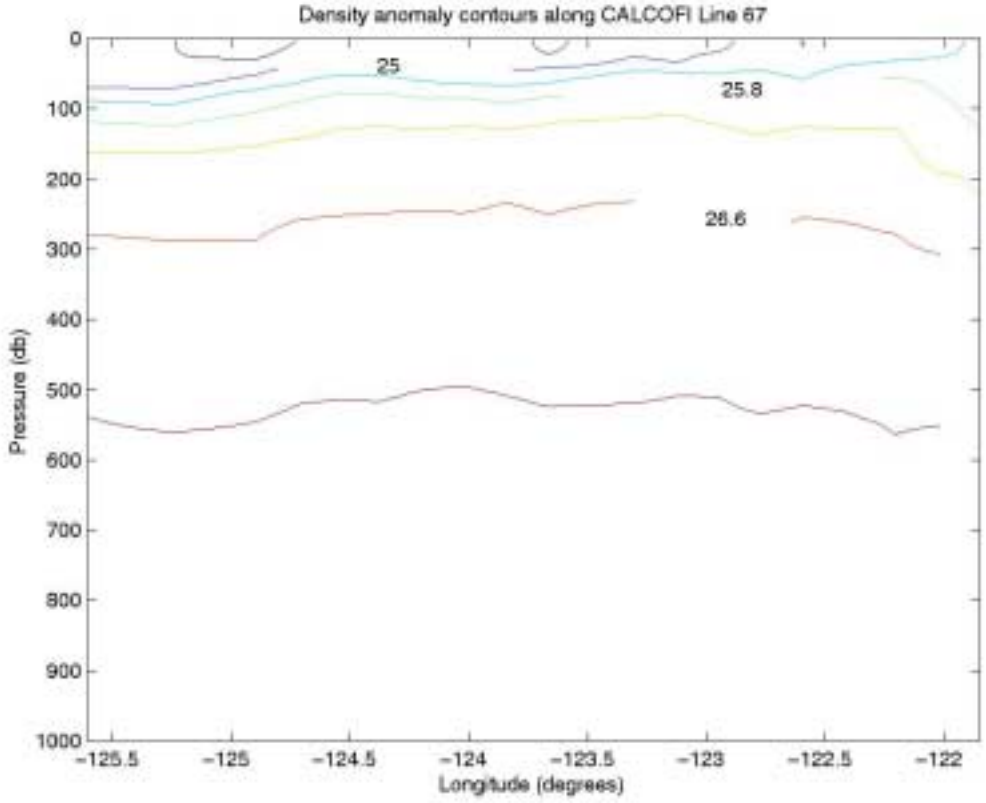

Figure 7. Density anomaly (kg/m^3) along CALCOFI Line 67

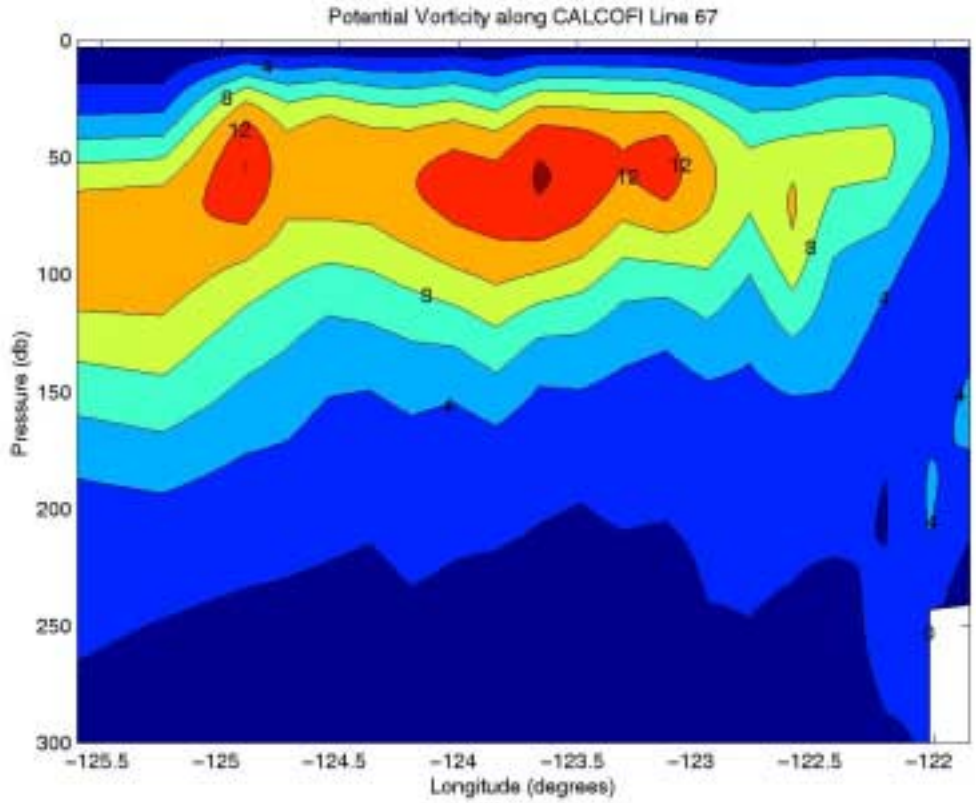

Figure 8. Potential vorticity, $(f/\rho)d\rho/dz$, (10^{-10} $m^{-1}s^{-1}$) along CALCOFI Line 67

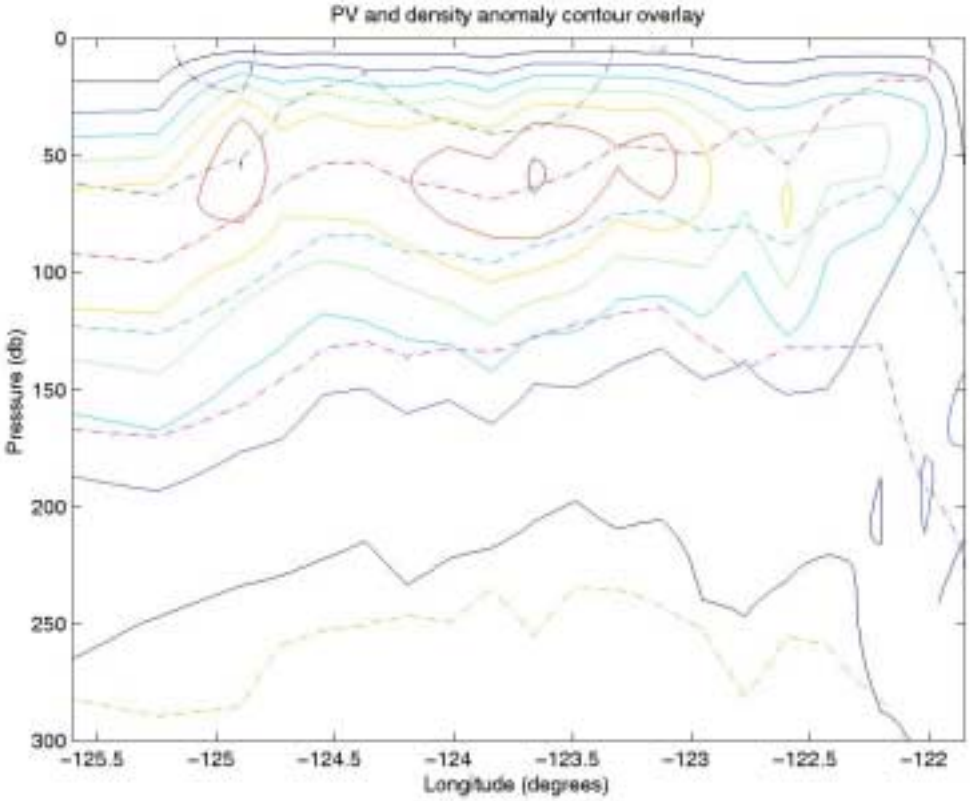

Figure 9. Potential vorticity (solid) and density anomaly (dashed).
Units are as in figures 7 and 8.

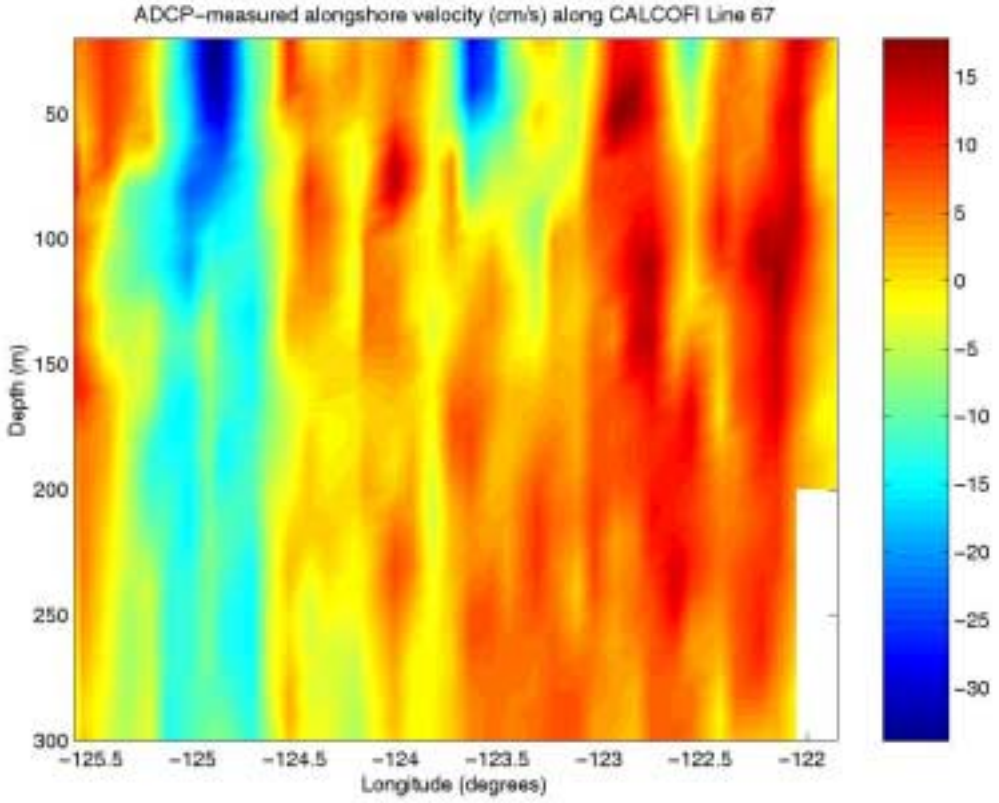
ADCP−measured alongshore velocity (cm/s) along CALCOFI Line 67
Depth (m)
50
100
150
200
250
300
−125.5
−125
−124.5
−124
−123.5
−123
−122.5
−122
Longitude (degrees)
15
10
5
0
−5
−10
−15
−20
−25
−30

Figure 10. Alongshore current (cm/s) as measured by ADCP along CALCOFI Line 67. Positive values indicate northward flow.